doi: 10.29382/eqs-2018-0137-3

Time-history responses on the surface by regularly distributed enormous embedded cavities: Incident SH-waves*

Mehdi Panji✉ and Saeed Mojtabazadeh Hasanlouyi

Department of Civil Engineering, *Zanjan Branch*, *Islamic Azad University*, *Zanjan* 58145-45156, *Iran*

Abstract The time-history responses of the surface were obtained for a linear elastic half-plane including regularly distributed enormous embedded circular cavities subjected to propagating obliquely incident plane SH-waves. An advanced numerical approach named half-plane time-domain boundary element method (BEM), which only located the meshes around the cavities, was used to create the model. By establishing the modified boundary integral equation (BIE) independently for each cavity and forming the matrices, the final coupled equation was solved step-by-step in the time-domain to obtain the boundary values. The responses were developed for a half-plane with 512 cavities. The amplification patterns were also obtained to illustrate the frequency-domain responses for some cases. According to the results, the presence of enormous cavities affects the scattering and diffraction of the waves arrived to the surface. The introduced method can be recommended for geotechnical/mechanical engineers to model structures in the fields of earthquake engineering and composite materials.

Keywords: circular cavities; half-plane BEM; time-history response; SH-wave; time-domain; wave propagation

1 Introduction

In today's modern world, the effect of irregularities and underground structures such as subsurface openings and cavities on the motions of ground surface is one of the most important topics in surface motion seismology in large cities (Aki, 1993). Therefore, the mentioned structures should be designed such that they can be sufficiently powered against static and dynamic loads. As a result, researchers in the field of geophysical and seismic prospecting are concerned with measuring and analyzing them, which requires detailed understanding of how the presence of these irregularities affects the surface motion. Moreover, the realistic applications of multiple cavities cover a wide range of problems in geotechnical and mechanical engineering. The analysis of underground structures and tunnels, especially in urban environments, energy transfer, and dam galleries, are instances of multiple cavities' applications in the field of geotechnical engineering. Additionally, the analysis of myriad cavities can be used for the evaluation of composite materials' behavior in mechanical engineering. These applications are developing with the rapid growth of sciences, for instance, the professional nano-technologies that introduces modern materials with enormous cavities for special applications in different fields of emerging engineering. Consequently, it is essential for geotechnical or mechanical engineers to utilize appropriate methods for obtaining more accurate responses. Technically speaking, there are different methods for the seismic analysis of the ground surface with cavities, including analytical, semi-analytical, experimental, and numerical methods (Sánchez-Sesma, 2002).

Numerous analytical and semi-analytical methods have been presented to study the scattering and diffraction of SH-waves by different types of heterogeneities, including cavities, since the mid-1940s. In most of these studies, a half-space is considered as the medium. In this regard, one (Mow and Pao, 1971) can refer to which presented an exact solution based on the wave-function expansion method for plane SH-wave propagation in an infinite elastic-domain containing a circular cavity. Some other studies (Lee, 1977; Datta and EI-Akily, 1978; Datta and Shah, 1982) subsequently presented similar solutions for the diffraction of SH-waves by a cylindrical cavity in the elastic half-plane. Within this period, Lee and Trifunac (1979) investigated the response of tunnels to incident SH-

* **Received** 11 March 2018; **accepted in revised form** 11 June 2018; **published** 24 August 2018.
✉ **Corresponding author. e-mail**: m.panji@iauz.ac.ir

waves using the series solution. In this study, the angle of wave incidence, stresses, and deformations near the tunnels were considered. Over the next few years, Liang et al. (2003, 2004) studied the presence of underground twin tunnels on the response of ground surface displacements and motion amplification subject to SV- and P-waves, respectively, using Fourier-Bessel series expansion method. In another study, using the method of wave function expansion, Balendra and Thambiratn (1984) obtained a closed-form of the dynamic response of two parallel circular cavities subjected to incident plane harmonic SH-waves. In fact, the popularity and high quality of the above-mentioned method led the researchers to use it frequently. Moreover, Lin and Liu (2002) proposed an analytical method to study the scattering of SH-wave around a circular cavity in a half-space. Similarly, Liang et al. (2007) examined the effect of a single cavity placed in a saturated poroelastic medium incident to SV-waves diffraction using the wave function series expansion solution. Using the same method, Smerzini et al. (2008) presented the results for an embedded circular cavity as well as lined tunnel subjected to SH-wave propagation from a seismic source along a parallel line to the axis of the cavity. Using the wave function expansion method, Luo et al. (2010) and Liang et al. (2010) investigated the dispersion of the antiplane and plane SH-waves due to the presence of an underground semi-circular cavity, respectively. Moreover, Luo et al. (2010) introduced a more accurate analytical method named "improved cosine half-range expansion" algorithm for a better performance in reduction of displacement residual errors. A few years later, Liu et al. (2014) proposed an analytical solution for the antiplane scattering of plane SH-waves by a circular cavity in an exponentially graded half-space obtained by the complex variable method and image technique. Recently, Liu et al. (2016) studied the scattering of SH-waves by a rectangular cavity in a half-space using an auxiliary circle method based on wave function expansions. Utilizing the wave function expansion method and image technique, a closed-form solution was obtained by Faik Kara (2016) based on the diffraction of plane harmonic SH-waves around a cylindrical cavity in a homogeneous, isotropic, and linear elastic infinite wedge.

A review of relevant literature shows that the problem of scattering waves interacting with a system of irregularities was officially proposed by Foldy (1984) for the first time. He considered the scattering of scalar waves in a random distribution of isotropic scatterers. Then, Lax (1951) extended the results to anisotropic scattering with the assumption that the scatterers were arranged randomly, partially, or completely. Furthermore, Twersky (1952) investigated the planar configuration of parallel cylinders in two-dimensional (2D) acoustic/electromagnetic multiple scattering. In this study, the effect of the greatest wavelength of the multiple scattered waves was derived for small radii compared to the wavelength using an integral equation approach. As a result, a criterion for the single scattering wave was presented for the model of two cylinders. Subsequently, Twersky (1962) studied the scalar multiple scattering of arbitrary heterogeneity using a three-dimensional (3D) model in which the amplitudes of many objects were presented in terms of related functions for the segregated object with the integral equation approach. The closed-forms were derived specially for two objects in this study. In addition, Varadan et al. (1978) investigated the multiple scattering of SH-waves using the *T*-matrix approach by applying randomly distributed infinite cylinders placed within a full-space model. Similarly, using the *T*-matrix method, Yang and Mal (1994) examined the scattering of SH-, P-, and SV-waves for randomly distributed parallel fibers. Some researchers estimated the dispersion and attenuation of elastic waves in the field of multiple scattering of elastic waves, one of which is Kikuchi (1981a). In this study, the apparent dispersion and attenuation of elastic waves for a plane strain model with uniformly distributed cracks subjected to the propagation of P-, SV-, and SH-waves were explored. In his next study, he developed the model of uniformly distributed inclusions using the wave function expansion method (Kikuchi, 1981b).

Due to the complexity and low flexibility of the analytical models for formulating complex geometric problems, the use of numerical methods is inevitable. On the other hand, due to the significant improvements of computers and computing devices, numerical methods have gained more attention in studies conducted in recent decades. The common numerical methods are divided into two general categories, including domain and boundary methods. In fact, there are different volumetric and boundary methods which can be used for the analysis of soil dynamics and wave propagation problems, including the finite-element method (FEM), finite-difference method (FDM), and boundary element method (BEM). The considered domain should be discretized and the energy absorber boundaries need to be defined to analyze the infinite and semi-infinite continuous media using FEM or FDM, thus increasing the complexity of the problem and leading to a longer analysis time. Based on the above

explanation, a parametric study performed by Alyagshi and Sandhu (1987) for the scattering of SH-waves in infinite spaces using the finite element eigenfunction method. Recently, Li and Song (2015) studied the longitudinal seismic response of tunnels under asynchronous P-, SV-, and SH-waves by FEM in the 3D mode. Moreover, Huang et al. (2017) examined the impact of the incident direction of SV- and SH-waves on 3D non-linear seismic responses of the long-lined tunnels using FEM. Additionally, Do et al. (2015) studied the response of segmental tunnel lining under seismic loading using a 2D FDM model.

With the help of BEM, one dimension of modeling diminishes and the Sommerfeld's radiation conditions of the waves at infinity can be automatically satisfied which becomes more clear when used for the analysis of various problems with infinite and semi-infinite boundaries (Beskos, 1987, 1997). As the basic study in this field, Wong and Jennings (1975) investigated the 2D scattering and diffraction of SH-waves for an arbitrary angle to irregular canyon-shaped topography, formulated using an integral equation and solved by numerical methods. Moreover, a boundary method was employed by England et al. (1980) to numerically solve the problem of scattering of SH-waves by a bounded surface cavity or arbitrary shape in a half-space. Additionally, Luco and de Barros (1994) presented the 2D response of a viscoelastic half-space subjected to harmonic-plane SH, P, SV, and Rayleigh waves using an indirect boundary integral method based on 2D Green's functions. In these studies, the full-plane BEM formulation is incorporated. It is inevitable to truncate the model from a full-space and discrete it in a distance far away from the desired zone in order to satisfy the stress-free conditions on the ground surface (Ahmad and Banerjee, 1988). Some studies have used full-plane modeling process to analyze the behavior of various types of topographic features and obtain site responses; these include works by Panji et al. (2011, 2016) in static mode, and also Parvanova et al. (2014a, 2015) in seismic mode. Furthermore, it is possible to use half-plane BEM formulation as the second method in order to model semi-infinite problems. Although the implementation of the formulation is more difficult in such an approach compared to the full-plane case, it does not need to discrete the ground surface and define the fictitious elements and, therefore, the models would be simpler. Several studies have been performed using the half-plane BEM in static mode, including Panji and Ansari (2017a). There are also several studies for seismic analysis in frequency-domain due to the propagation of incident SH-waves, including Dravinski (1982, 1983), Ohtsu and Uesugi (1985), Reinoso et al. (1993), and Ausilio et al. (2008). Liang and Liu (2009) investigated the plane SV-waves' diffraction in a poroelastic half-space by a cavity using indirect boundary integration equation method. However, few studies have been conducted by implementing the half-plane BEM in the time-domain, including Rice and Sadd (1984), Hirai (1988), and Belytschko and Chang (1988). Moreover, in the field of seismic analysis, Panji (2013), Panji et al. (2013a, b; 2014a, b) and, recently, Panji and Ansari (2017) can be mentioned.

According to the methods described above and by reviewing previous studies in the case of multiple irregularities, it can be observed that Benites et al. (1992, 1997), and Yomogida et al. (1997) investigated antiplane/plane strain elastic wave scattering for the system with many cavities. The models have been presented in full-space and half-space subjected to the plane SH-, P- and SV-waves using an indirect boundary integral equation approach. The results of these studies demonstrated that amplification or de-amplification strongly depends on the position of the line source relative to the area where the multiple cavities are located. Moreover, the debilitation of the direct wave and the duration of the time-history responses increase significantly when the line source is very close to or inside the heterogeneous region, compared to the case in which it is outside. Using a frequency-domain BEM, Kattis et al. (1999) studied the multiple scattering of elastic waves in a row of piles inside an elastic half-space model subjected to a point harmonic surface load. They showed that the tranches are consistently more effective in the reduction of the surface motion compared to the pile barrier. In another study, Antonio and Tadeu (2001) investigated the 3D scattering of the elastic waves for the case of two cylindrical cavities within a full-space using a BE formulation, clearly demonstrating the significance of the existence of the second cavity upon their results. Furthermore, Wang and Liu (2002) performed a dynamic analysis of multiple circular cavities subjected to SH-waves in a half-plane using an analytical solution. Robert et al. (2004) investigated 2D resonant elastic scattering by a finite number of close cylindrical cavities subjected to plane harmonic P/SV-waves using the scattering matrix approach. In their study, the numerical results showed a comparison between the interactions of empty or fluid-filled cavities. Wang and Sudak (2007) analyzed the scattering of incident plane P/SV-waves affected by elastic circular cylinders in full-space mode using an analytical multipole expansion

method. They illustrated the importance of multiple scattering domination on the response due to the impact of incident plane SV-waves. Avila-Carrera et al. (2008) investigated the 2D multiple scattering of elastic waves of regularly distributed cylindrical obstacles subjected to an incident antiplane shear wave using the superposition of cylindrical wave functions. The results were obtained for various cases of cavities and inclusions. Using a direct boundary integral equation (BIE) approach, Dravinski and Yu (2011) studied the scattering of plane harmonic SH-waves by an arbitrary number of multiple inclusions within an elastic half-space model. Their results clearly showed the importance of the interactions between inclusions for a wide range of parameters such as the nature of incident waves, geometry of the model, and number of inclusions. Furthermore, using BIEM approach, Parvanova et al. (2013) examined the dynamic behavior of a finite-sized elastic solid with multiple cavities and inclusions. Recently, Parvanova et al. (2014) utilized direct BEM with sub-structuring capabilities and obtained the seismic response of unlined and lined tunnels, as well as multiple buried inclusions within an elastic homogeneous half-plane. The horizontally polarized waves (SH, SV, P and Rayleigh) were assumed propagation in the half-plane medium in the frequency-domain. Finally, Sheikhhassani and Dravinski (2014) examined the scattering of a plane harmonic SH-wave by multiple layered inclusions using a direct BIE approach.

As the literature review shows, the multiple scattering of waves due to the presence of cavities has not yet been directly analyzed in the time-domain. Therefore, in the present case study, a half-plane time-domain BEM is applied to obtain the time-history responses of the surface including regularly distributed enormous embedded circular cavities subjected to propagating incident plane SH-waves. After developing the method to solve the problem of multiple cavities and implementing it in the general algorithm of DASBEM (Panji et al., 2013b), a verification example is analyzed in order to confirm the method and prepared algorithm. Then, in the form of a numerical study, the time-domain responses of the ground surface as time-history responses were obtained for a linear elastic half-plane with enormous embedded cavities. The models are extended from a single cavity to 512 cavities. Finally, the amplification patterns of the surface are presented for some of the cases. The main objectives of the this paper are presenting the ability and efficiency of the method for the transient analysis of problems with complex geometry and showing some graphs to contribute to the sciences of geotechnical earthquake engineering and composite materials' behavior.

2 Statement of the problem

A linearly elastic homogeneous and isotropic half-plane medium is considered, as shown in Figure 1. The equation of motion for the antiplane strain model is as follows

$$\frac{\partial^2 u(x,y,t)}{\partial x^2}+\frac{\partial^2 u(x,y,t)}{\partial y^2}+b(x,y,t)=\frac{1}{c^2}\frac{\partial^2 u(x,y,t)}{\partial t^2}, \quad (1)$$

where $u(x, y, t)$ and $b(x, y, t)$ are out-of-plane displacement and body force at point (x, y) and current time t, respectively. Moreover, c is the shear-wave velocity given by $\sqrt{\mu/\rho}$ in which μ is the shear modulus and ρ is the mass density. The singular solution of equation (1), with no regard to any boundary conditions, gave full-plane fundamental solutions Israil and Banerjee (1990a, b). Nevertheless, for a 2D antiplane semi-infinite medium, equation (1) was solved with the following boundary condition

$$\mu\frac{\partial u(x,y,t)}{\partial \mathrm{n}}\bigg|_{y=0}=0, \quad (2)$$

where n is the normal vector that is perpendicular to the ground surface. Simultaneously, the singular solution of equations (1) and (2) represented the half-plane fundamental solution Panji et al. (2013b). As depicted in Figure 1, a system of multiple cavities is intended within an elastic half-plane subjected to different angles of incident SH-waves of the Ricker type (Panji, 2013a, b). Γ with the subscript 11 to 1N represents the number of cavities' boundary from the first to infinity in the first row. The adjacent cavities are placed in regular rows and columns relative to each other. b and d denote the radius and depth of cavities, respectively which equal d=1.5b. The center-to-center distance of cavities is marked by e and considered to be 3b. The outward unit normal vector

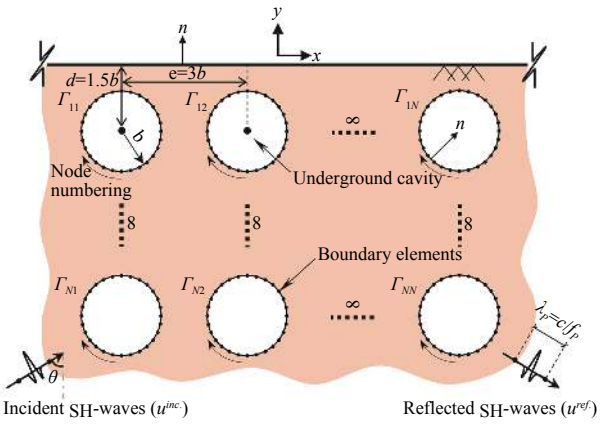

Figure 1 The problem geometry of the multiple cavities within an elastic half-plane subjected to incident SH-waves

for all of the surfaces is denoted by $\vec{n}$ and the angle of incidence waves is presented by θ.

3 Time-domain half-plane BEM

This method utilizes the technique of wave source image (Panji, 2013b) to the ground surface and, by satisfying the boundary conditions on it, exclusively concentrates the meshes around the cavity. Details on this method are presented in the following section.

3.1 BIE for wave scattering

The weighted residual integral is applied on equation (1). The volumetric integral terms are eliminated using boundary methods. Then, the contributions of the initial conditions and body forces are ignored. The direct BIE in the time-domain is obtained by defining the time-convolution integral as follows (Brebbia and Dominguez, 1989; Dominguez, 1993):

$$c(\xi)u(\xi,t)=\int_{\Gamma}\left\{\int_{0}^{t}\left[u^{*}(x,t;\xi,\tau)q(x,t)-q^{*}(x,t;\xi,\tau)u(x,t)\right]\mathrm{d}\tau\right\}\mathrm{d}\Gamma(x)+u^{\mathrm{ff}}(\xi,t), \tag{4}$$

where the free field displacement of the ground surface is u^{ff} (without surface irregularities). For multiple cavities,

$$c(\xi)u(\xi,t)=\sum_{C=1}^{NN}\left[\int_{\Gamma_C}\left\{\int_{0}^{t}\left[u^{*}(x,t;\xi,\tau)q(x,t)-q^{*}(x,t;\xi,\tau)u(x,t)\right]\mathrm{d}\tau\right\}\mathrm{d}\Gamma_C(x)+u^{ff}(\xi,t)\right]_C, \tag{5}$$

in which NN represents the number of cavities. The total displacement of the multiple cavities is obtained by solving equation (5). Once equation (5) is solved, it is possible to obtain the displacements at any point m in Ω,

$$u^{m}(\xi,t)=\sum_{C=1}^{NN}\left[\int_{\Gamma_C}\left\{\int_{0}^{t}\left[u^{*m}(x,t;\xi,\tau)q(x,t)-q^{*m}(x,t;\xi,\tau)u(x,t)\right]\mathrm{d}\tau\right\}\mathrm{d}\Gamma_C(x)+u^{ff.m}(\xi,t)\right]_C, \tag{6}$$

where u^{*m} and q^{*m} are half-plane displacement and traction fundamental solution for each internal point, respectively. Also, $u^{ff.m}$ is considered as free-field displacements that should be recalculated in this step.

4 Numerical implementation

To solve equation (5) and obtain the field variables, the time-axis and geometric boundary of the body must be discretized. No approximation is involved in this equation before the discretization and it is an exact solution. As will

$$c(\xi)u^{N}(\xi)=\sum_{C=1}^{NN}\left\{\sum_{n=1}^{N}\int_{\Gamma_C}\left(\begin{array}{c}\left[U_1^{N-n+1}(x,\xi)q^{n}(x)+U_2^{N-n}(x,\xi)q^{n}(x)\right]-\\ \left[Q_1^{N-n+1}(x,\xi)u^{n}(x)+Q_2^{N-n}(x,\xi)u^{n}(x)\right]\end{array}\right)\mathrm{d}\Gamma_C(x)+u^{ff.N}(\xi)\right\}_C \tag{7}$$

where U_1^{N-n+1} and U_2^{N-n+1} are the half-plane displacement time-convoluted kernels, respectively; Q_1^{N-n+1} and Q_2^{N-n+1}

$$c(\xi)u(\xi,t)=\int_{\Gamma}\left\{\int_{0}^{t}\left[u^{*}(x,t;\xi,\tau)q(x,t)-q^{*}(x,t;\xi,\tau)u(x,t)\right]\mathrm{d}\tau\right\}\mathrm{d}\Gamma(x), \tag{3}$$

where u^* denotes the fundamental solution of the time-domain half-plane displacement and q^* denotes the fundamental solution of the time-domain half-plane traction. In addition, u and q are the displacements and tractions of the boundary, respectively. $\Gamma(x)$ denotes the boundary of body and x is the position vector. Moreover, u^*q and q^*u denote the Riemann-convolution integrals and $c(\xi)$ is the geometry coefficient (Panji, 2013b). In an infinite space, the free field displacement is identical to the incident wavefield $u^{\mathrm{inc}}(x,\ t)$ because of the radiation condition. In addition, a reflected wave field $u^{\mathrm{ref}}(x,\ t)$ must be considered to the reverse phase of incident wave in order to obtain the free-field displacement by summing the incident and reflected wavefield. Accordingly, BIE [equation (3)] is modified as (Kawase, 1988; Hadley et al., 1989)

equation (4) can be rewritten as equation (5)

including the surface (y=0) of the ground. Accordingly, the following modified equation is used in which $c^m(\xi)$ is equal to 1 for internal points

be shown, in order to carry out the temporal integration, the analytical process is elaborated and the numerical procedure is performed for the spatial integration.

4.1 Temporal integration

For the temporal integration, the time interval from 0 to t is divided into N equal increments with Δt, that is $t=N\Delta t$. Within each time-step, the field variables can be assumed to remain linearly. After temporal integrations, the time-convoluted BIE will be rewritten as equation (7):

are the half-plane traction time-convoluted kernels corresponding to the forward and backward time-nodes within a time-step, respectively that have been condensed in the closed-form. Also, u^N and $u^{ff.N}$ stand for boundary displacement and free-field displacement at time $t=N\Delta t$, respectively. The half-plane displacement and traction time-convoluted kernels for antiplane elastodynamics can be found in Panji et al. (2013b, 2014a).

4.2 Spatial integration

The boundary of the domain was discretized with isoparametric quadratic elements in order to numerically accomplish the spatial integration. Subsequently, all quantities such as geometry and field variables are given in terms of nodal variables as follows

$$x_i(\kappa) = N_a(\kappa)\, x_{ia}, \tag{8}$$

$$f(x(\kappa)) = N_a(\kappa)\, f_a, \tag{9}$$

in which f stands for the displacement and traction, i=1, 2; α=1, 2, 3; $N_a(\kappa)$ represent quadratic shape functions, and κ denotes the local intrinsic coordinates of the elements. With the spatial discretization, equation (7) is rewritten as

$$c(\xi)u^N(\xi) = \sum_{C=1}^{NN}\left\{\sum_{n=1}^{N}\sum_{m=1}^{M}\left[\begin{array}{l}\int_{\Gamma_m}\left[U_1^{N-n+1}(x(\kappa),\xi)+U_2^{N-n}(x(\kappa),\xi)\right]N_\alpha(\kappa)|J|\,\mathrm{d}\kappa q_\alpha^n - \\ \int_{\Gamma_m}\left[Q_1^{N-n+1}(x(\kappa),\xi)+Q_2^{N-n}(x(\kappa),\xi)\right]N_\alpha(\kappa)|J|\,\mathrm{d}\kappa u_\alpha^n\end{array}\right] + u^{ff.N}(\xi)\right\}_C \tag{10}$$

where M represents the total number of BEs for each cavity, Γ_m indicates the portion of the boundary to which element 'm' belongs and J is the Jacobian of transformation that can be obtained from the following equation

$$J_i = \frac{\partial N_\alpha(\kappa)}{\partial \kappa} x_{i\alpha}, \tag{11}$$

4.3 Time-stepping algorithm

After forming the spatial integration of equation (10) for each boundary node, the equation is obtained in the matrix form as

$$\sum_{C=1}^{NN}\left[\sum_{n=1}^{N}\boldsymbol{H}^{N-n+1}\boldsymbol{u}^n\right]_C = \sum_{C=1}^{NN}\left[\sum_{n=1}^{N}\boldsymbol{G}^{N-n+1}\boldsymbol{q}^n + \boldsymbol{u}^{ff.N}\right]_C, \tag{12}$$

in which $\boldsymbol{H}^{N-n+1}$ and $\boldsymbol{G}^{N-n+1}$ are the matrices whose elements are obtained by integration over the BEs. Also, $\boldsymbol{u}^n$ and $\boldsymbol{q}^n$ are vectors of boundary nodal quantities at time-step n. In this particular problem, term $\boldsymbol{G}^{N-n+1}\boldsymbol{q}^n$ is equal to zero, because there is no traction on the boundary of the cavities. Therefore, the matrix form of equation (12) would be as follows

$$\left[H^1H^2H^3\cdots H^{NN}\right]\begin{bmatrix}u^1\\u^2\\u^3\\\vdots\\u^{NN}\end{bmatrix} = \begin{bmatrix}R^1\\R^2\\R^3\\\vdots\\R^{NN}\end{bmatrix} + \begin{bmatrix}u^{ff.1}\\u^{ff.2}\\u^{ff.3}\\\vdots\\u^{ff.NN}\end{bmatrix}, \tag{13}$$

in which $u^{ff.1}$ to $u^{ff.NN}$ represent the free-field responses of the first to NNth cavity, and R^1 to R^{NN} are related to the past time-history of the first to NNth cavity. By applying the boundary conditions to the nodes, ordering the unknown parameters on the left side, and considering H^1 to H^{NN} as $\boldsymbol{A}$, u^1 to u^{NN} as $\boldsymbol{X}^N$, R^1 to R^{NN} as $\boldsymbol{R}^N$ and $u^{ff.1}$ to $u^{ff.NN}$ as $\boldsymbol{u}^{ff.N}$, equation (13) can be rewritten in the compact form as follows

$$[\boldsymbol{A}]\,\boldsymbol{X}^N = \boldsymbol{R}^N + \boldsymbol{u}^{ff.N}, \tag{14}$$

where $\boldsymbol{X}^N$ is the vector of unknown variables and $\boldsymbol{R}^N$ involves the effects of past dynamic history on the current time-node N as

$$\boldsymbol{R}^N = \sum_{C=1}^{NN}\left[\sum_{n=1}^{N-1}(-\boldsymbol{H}^{N-n+1}\boldsymbol{u}^n)\right]_C, \tag{15}$$

Solving equation (14) gives all boundary unknowns at each time-step. Once equation (14) is solved, it is possible to obtain the displacements at any internal point m in the domain. Then

$$\boldsymbol{u}^{N.m} = \sum_{C=1}^{NN}\left[\sum_{n=1}^{N}(-\boldsymbol{H}^{\langle N-n+1\rangle.m}\boldsymbol{u}^n) + \boldsymbol{u}^{ff.N.m}\right]_C, \tag{16}$$

where $\boldsymbol{u}^{N.m}$ and $\boldsymbol{u}^{ff.N.m}$ are displacement and free-field response at any arbitrary internal point, respectively. Moreover, $\boldsymbol{H}^{\langle N-n+1\rangle.m}$ is the matrix whose elements depend on the location of internal points and boundary nodes.

5 Validation example

The proposed formulation is implemented in a general half-plane BEM code, previously named as DASBEM. To illustrate the applicability and accuracy of this algorithm in the analysis of the dynamic displacements of multiple cavities problems, four cavities are considered in a linear elastic half-plane subjected to incident SH-waves. Figure 2 illustrates the normalized displacement amplitude of the ground surface involving four cavities embedded in the depth of 1.5b marked by d. The dimensionless frequencies ($\eta=\omega b/\pi c$) of 0.5, 1.0, 1.5, and 2.0 are considered where ω represents the angular frequency of the wave. b and c also denote the radius of the cavities and shear-wave velocity of the medium, respectively. The normalized displacement

amplitude (NDA) is defined as

$$\mathrm{NDA}=\frac{\text{Fourier amplitude of the total motion of ground surface obtained by BEM for a defined frequency}}{\text{Fourier amplitude of the incident motion for a defined frequency}} \tag{17}$$

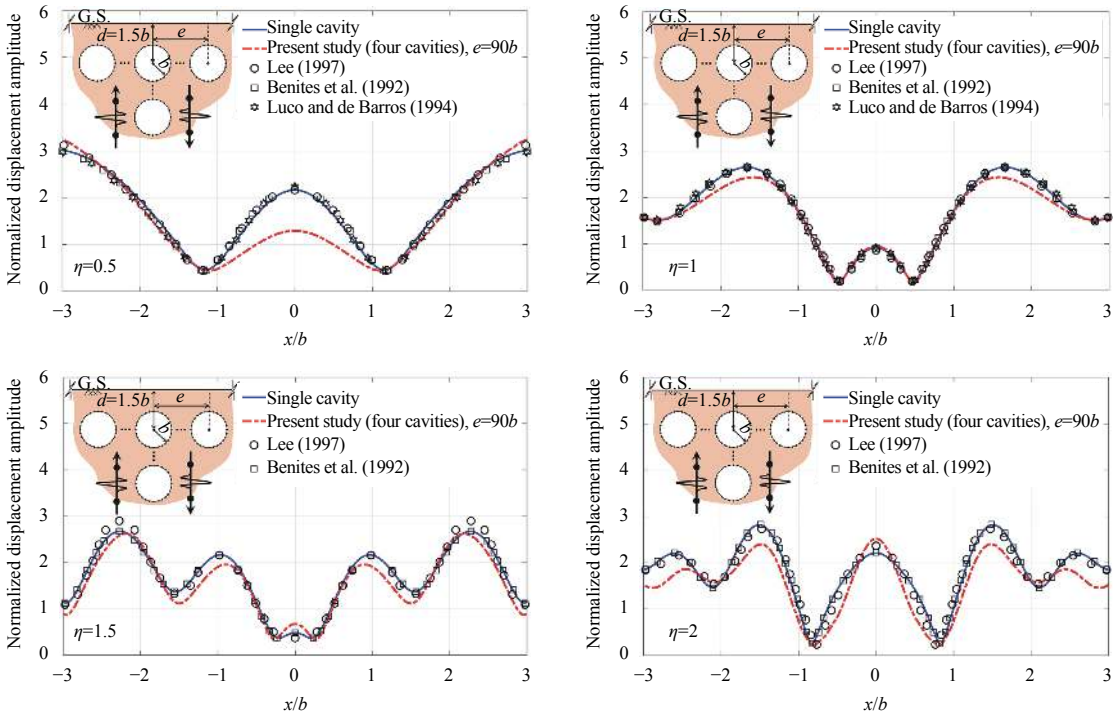

Figure 2 Normalized displacement amplitude of the ground surface versus x/b for the model of four cavities with the radius of b in the depth of d=1.5b and e=90b subjected to SH-waves and the incident angle of θ=0° for different dimensionless frequencies

The published solutions of this problem were presented for different η values by Lee (1977) using an analytical solution and two other solutions were presented by Benites et al. (1992) and Luco and de Barros (1994) using indirect BEM. All of the cavities have a circular shape and the same radius. According to Figure 2, the adjacent cavities are placed in the horizontal and vertical distance of 90b from the reference cavity that has been defined by the ***e*** parameter. In order to solve this example, two types of model were prepared for the single and four cavities that have been established by the half-plane time-domain BEM. In these models, the shear-wave velocity and density are equal to 1000 m·s^{-1} and 1 kg·m^{-3}, respectively. The predominant frequency and maximum amplitude of SH-wave of the Ricker wavelet type are equal to 3 Hz and 0.001 m and the time-shifting parameter is equal to 2.4 and 74.4 s for single and multiple cavities, respectively. The problem is solved by using 600 and 4750 time-steps with Δt of 0.01 and 0.0238 s for the single and multiple cavities, respectively. Additionally, the number of BEs considered for each cavity is equal to 126 and, in total, 504 for 4 cavities in the model. The numerical procedure is implemented using MATLAB software.

Comparison of the results for different scenarios with the mentioned solutions indicates a good agreement for single and multiple cavities. Moreover, it is concluded that by increasing the ***e*** parameter in horizontal and vertical directions, more compliance will be achieved in results.

6 Time-history responses

In order to view the general patterns of responses in the time-domain, Figure 3 is presented for the single circular cavity, indicating the scattering and diffraction of SH-waves. All the parameters are considered with the same values as those of the previous section, and the responses for this model are shown in the range of 3b to –3b on the ground surface. Despite the responses of the frequency-domain, the effect of reflection and diffraction of the waves can only be observed in the time-domain. Furthermore, the angles of incident SH-waves are 0°, 30°, 60°, and 90°, respectively. The circular shape of the cavities has been selected for research purposes for convenience and suitability. The consideration of the 3b distance between the centers of cavities in each row and column is an initial assumption for the regular distribution of the cavities in the

half-plane medium and providing the possibility to investigate the distribution of incident waves between near cavities in the same arrangement. Additionally, all of the computed time-history responses are flipped vertically in order to provide a better visibility of their features. The scattering and diffraction of the incident SH-waves by 1, 2, 8, 32, 128, and 512 cavities are demonstrated in the following examples.

According to the time-domain responses of the ground surface illustrated in Figure 3, when the waves are applied

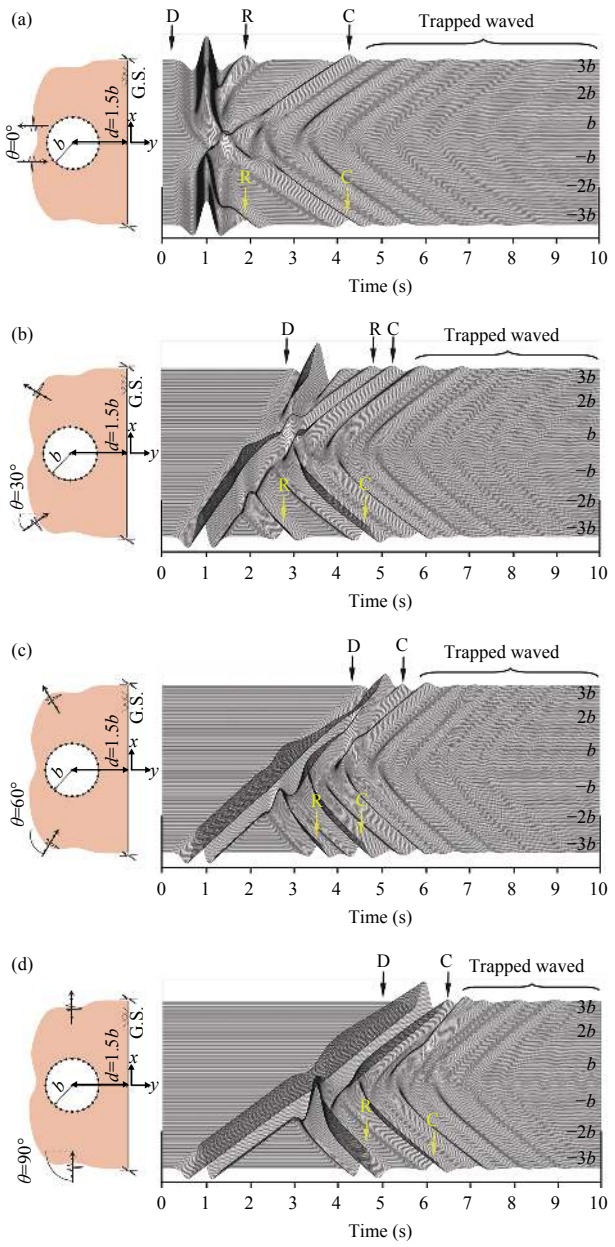

Figure 3 Time history responses of the ground surface and the procedure of SH-waves dispersion with time, for the model of one circular cavity embedded in the depth of 1.5*b* and the incident angle of (a) θ=0°, (b) θ=30°, (c) θ=60° and (d) θ=90°

to the models, some parts of the scattered waves directly encounter the ground surface, while some parts hit the cavity and are then reflected. Due to the diffraction and sliding of the incident waves on the boundary of the cavity, some parts are creeped around the cavity where the incidence direction is perpendicular to the unit normal vector (Keller, 1962). Based on the given description, three stations are marked on Figure 3, with D, R, and C, representing the direct, reflected, and creeped phases of the incident SH-waves, respectively. Furthermore, some part of these waves is trapped between the ground surface and the top boundary of the cavity, thus shaking up the diagram after C station in the time-line. If the number of cavities were more than one, the phenomenon of the trapped waves would occur with more intensity between cavities and the ground surface, since increasing the number of cavities affects the increment of severity and leads to more complexity in the results. In the case of vertically propagating incident waves, the symmetry of responses is maintained and the small amplitudes of displacement exist inside the position of cavity, because attenuation and time-delay occur in direct waves where the cavity is located and the field is aptitude to diffraction. Hence, the amplitudes of the reflected and creeped phases are smaller compared to the those of the direct incidence.

In the case of two cavities (Figure 4), the obtained time-history responses are slightly more complicated but can still distinguish the different phases of emitted waves such as multiple reflections among the cavities and the ground surface and the creeped phase upon the boundary of the cavities. The subscripts 1 and 2 indicate the relative stations to the first and second cavities, respectively. When the incidence waves propagate vertically, the time-history response indicates the same arrivals, clearly depicting the dispersion and reflection of the waves due to the presence of each cavity. By comparing the results of single and two cavities, it is concluded that, in the cases where the wave front is inclined, the positions of the R and C stations on the opposite side of the incoming waves gradually move close to each other regardless of the disruption in the symmetry of results. This occurs by increasing the angle of the incident waves. Hence, based on Figure 4, in cases where the incidence angles are greater than 30°, only the C station is visible. When the incidence angle is perfectly horizontal, the obtained amplitude of the reflected phase is higher than double that of the creeped phase, while for other modes, the amplitudes of R and C phases are almost identical. Likewise, the results for eight cavities are depicted in Figure 5 in which the transition of the waves is highlighted for each row of the cavities when the propagation angle of the applied waves is perpendicular to the

ground surface. In this model, the range of the ground surface is increased from –7b to 7b because a wider scope is covered by the cavities. It is necessary to mention that the complexity of the time-history responses for a greater number of cavities makes it very difficult to determine the individual phases. Therefore, hereinafter, only the general features of the scattered waves are mentioned on the time-domain responses. The computed time-domain results for the model of 32, 128, and 512 cavities are shown in Figures 6 to 8, respectively.

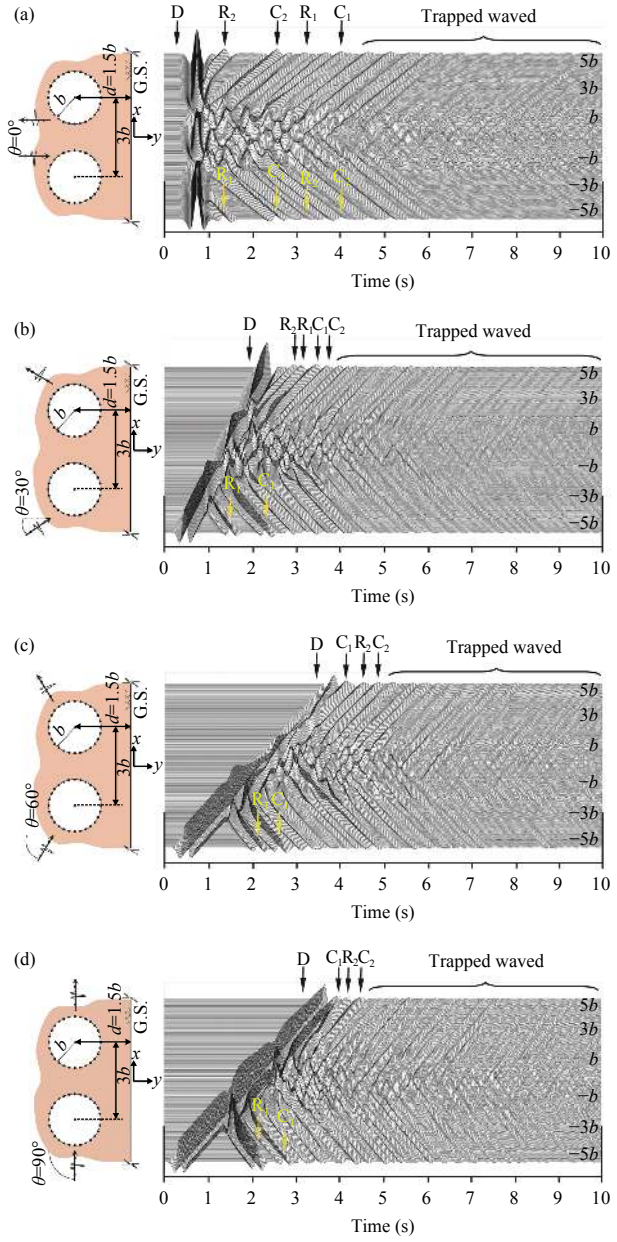

Figure 4 Time-history responses of the ground surface and the procedure of SH-wave dispersion with time, for the model of two circular cavities embedded in the depth of 1.5b and the incident angles of (a) θ=0°, (b) θ=30°, (c) θ=60°, and (d) θ=90°

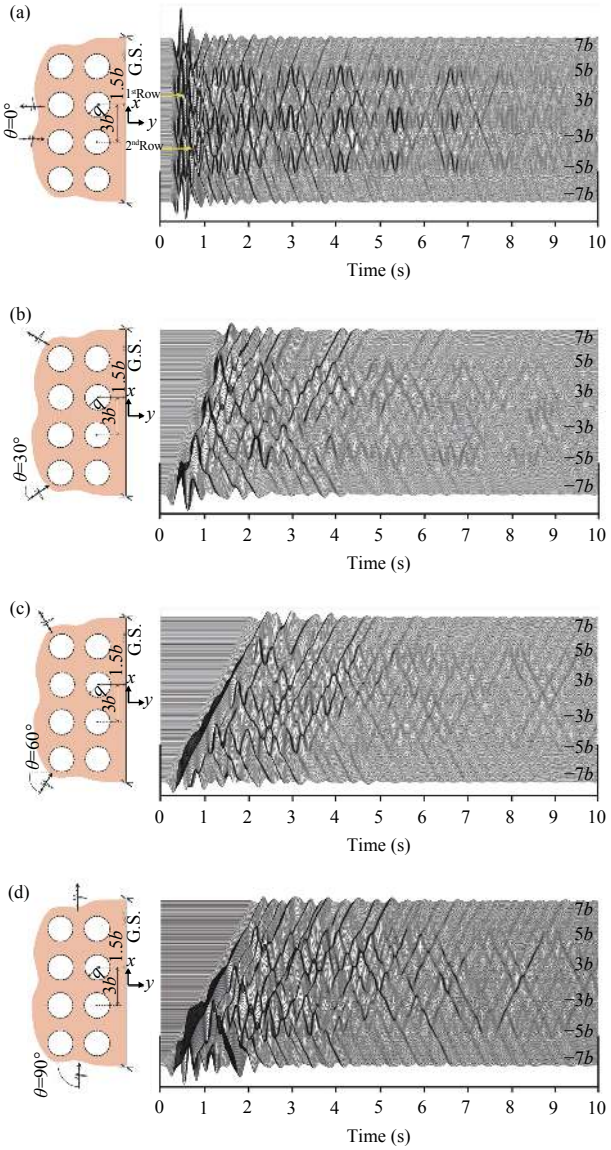

Figure 5 Time-history responses of the ground surface and the procedure of SH-waves dispersion with time, for the model of eight circular cavities embedded in the depth of 1.5*b* and the incident angles of (a) θ=0°, (b) θ=30°, (c) θ=60°, and (d) θ=90°

According to Figures 6 to 8, when the number of cavities increases, extreme complications are observed in the computed time-history response. In fact, it is because of the multiple reflections of the incident waves between the boundaries of the cavities. Despite the complexity of the time-history responses for different scenarios, they are helpful in understanding the comportment of incident SH-waves' diffraction in cases where the wave front is inclined or parallel to the horizon. In models with a large number of cavities, particularly in the models of 128 and 512 cavities for which the computed time-history responses have immense details, more time-line is required to achieve the full attenuation of the trapped waves. Hence,

for a better and more accurate display of the time-domain results, the time-line has been slightly shortened to show the precise features of the waves scattering in these cases.

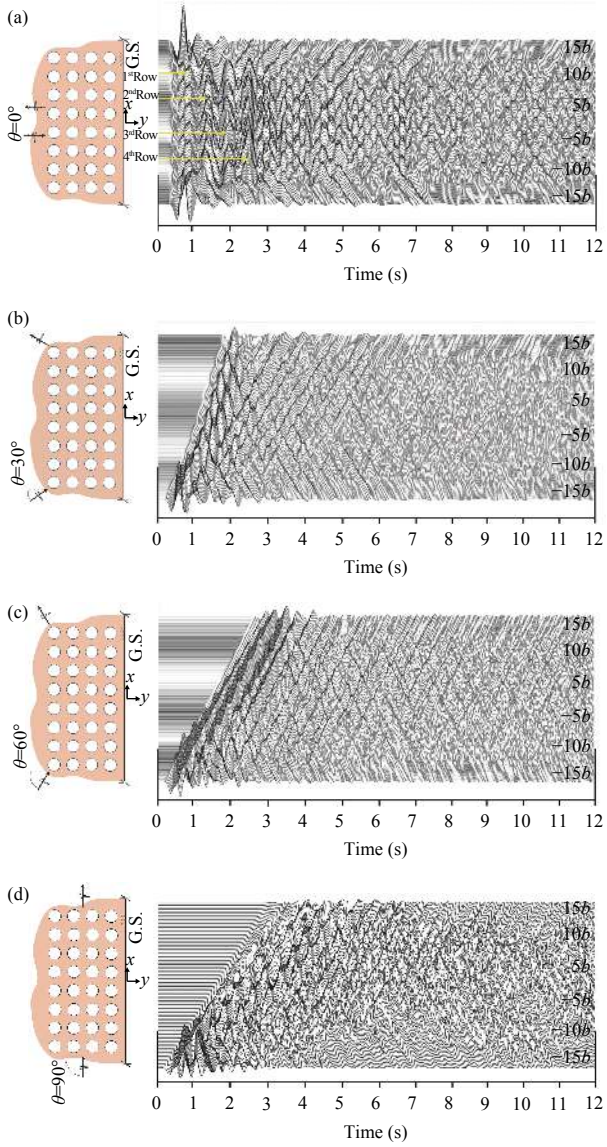

Figure 6 Time-history responses of the ground surface and the procedure of SH-waves dispersion with time, for the model of 32 circular cavities embedded in the depth of 1.5*b* and the incident angles of (a) θ=0°, (b) θ=30°, (c) θ=60°, and (d) θ=90°

7 Amplification patterns

Observing the general pattern of the surface displacement and its behavior under seismic forces is only possible in the frequency-domain, and Figures 9 to 11 are presented for this purpose. The amplification ratio of the ground surface is illustrated in the ranges of 5*b* to –5*b*, 10*b* to –10*b*, and 15*b* to –15*b*, versus dimensionless frequencies.

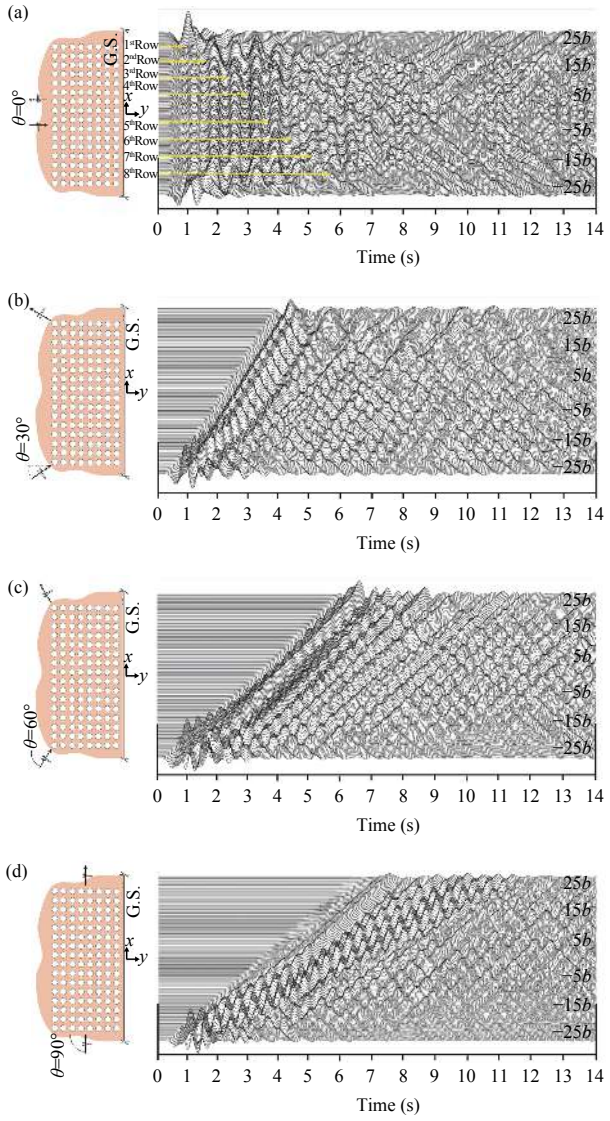

Figure 7 Time-history responses of the ground surface and the procedure of SH-waves dispersion with time, for the model of 128 circular cavities embedded in the depth of 1.5*b* and the incident angles of (a) θ=0°, (b) θ=30°, (c) θ=60°, and (d) θ=90°

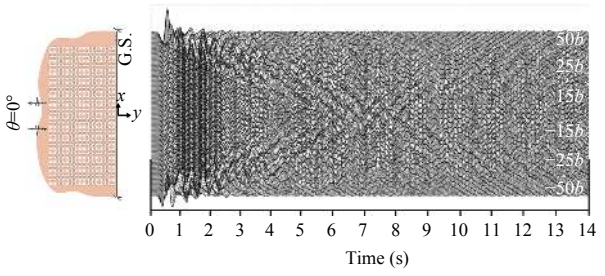

Figure 8 Time-history responses of the ground surface and the procedure of SH-waves dispersion with time, for the model of 512 circular cavities embedded in the depth of 1.5*b* and the incident angle of θ=0°

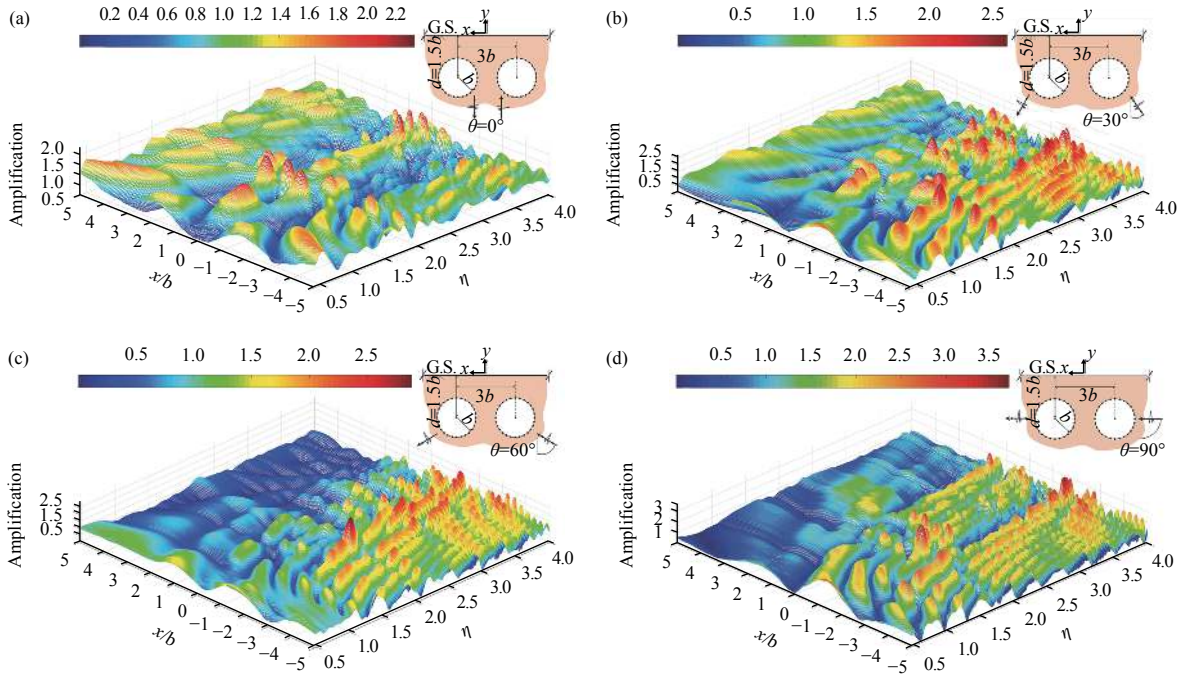

Figure 9 3-D amplification of the ground surface versus different dimensionless frequencies for the model of two circular cavities subjected to SH-waves and the incidence angles of (a) θ=0°, (b) θ=30°, (c) θ=60°, and (d) θ=90°

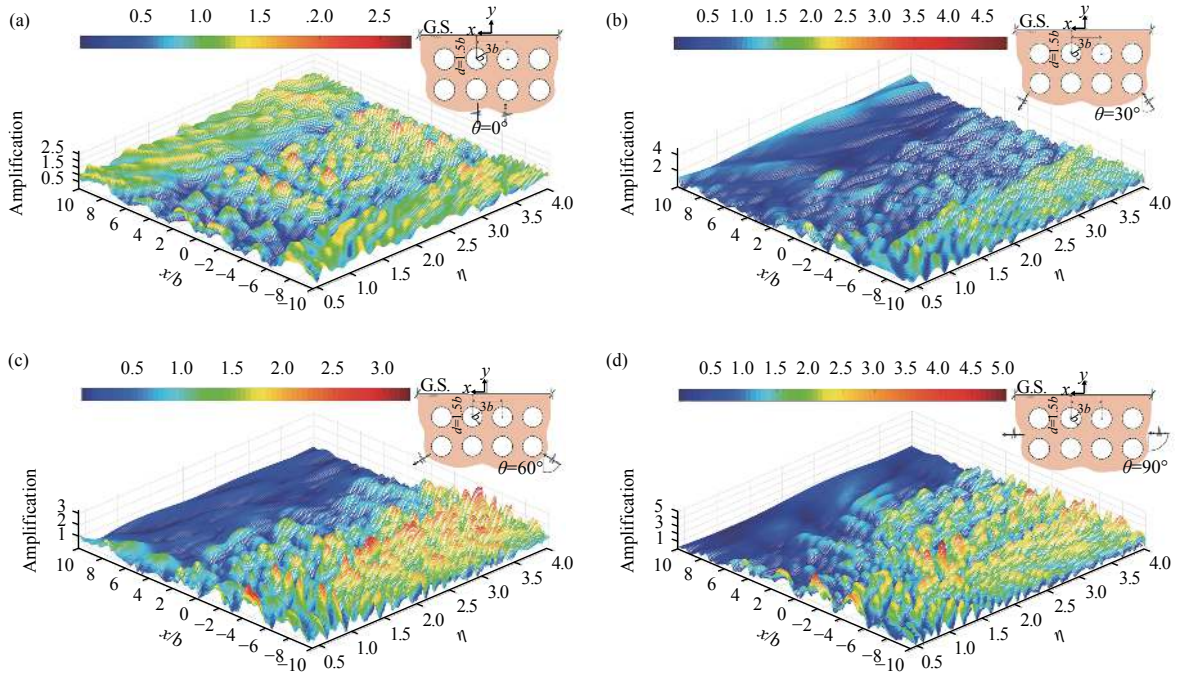

Figure 10 3-D amplification of the ground surface versus different dimensionless frequencies for the model of eight circular cavities subjected to SH-waves and the incidence angles of (a) θ=0°, (b) θ=30°, (c) θ=60°, and (d) θ=90°

These results are derived for the models of 2, 8, and 32 cavities, respectively, within an elastic half-plane. The amplification parameter is defined as the ratio of ground response amplitude to the free-field motion. For the models of 2 and 8 cavities, the results are presented for the different angles of incident SH-waves, whereas for the model of 32 cavities, only the vertical incidence is considered.

As can be seen in Figures 9 to 11, increasing the number of cavities leads to an increase in amplification in all cases. When the propagation of the incident SH-waves is

perpendicular, the results are symmetric. It may be a little difficult to recognize the symmetry in the 3-D plots because of their rotation. For this reason, Figures 12 to 14 are presented for a precise view. According to the results, in the models of 2 and 8 cavities, when the angle of incident waves is increased, the amplifications are decreased on the side away from the entrance wave front and increased on the opposite side. In other words, the cavities play the role of a guard trench against the wave front and do not allow a significant impact behind the cavities. This means that the presence of cavities in front of the incident waves leads to the amplification and compression of the scattered waves and, conversely, de-amplification on the other side. In other references (Trifunac, 1973), this effect has been referred to as the *shadow zone*. Because of this phenomenon, for the models with more underground cavities, de-amplification is clearer in the opposite direction of the wave front. For the amplification patterns of the 8-cavity model, when the angle of wave front is 30°, the volume of the reflected waves is higher than that of crawled waves. Therefore, a greater part of the wave is reflected and the waves have a lower chance to reach the ground surface from the spaces between the cavities. Nevertheless, when the wave front angle is 60° and 90°, waves can crawl around the cavities and reach the ground surface easier than the previous mode.

Figures 12 to 14 represent the precise view of the incident angle effect, especially on the seismic behavior of the surface. Because of the complexity of diagrams for a large number of cavities, only the results of 2, 8, and 32 cavities are presented separately for the different dimensionless frequencies.

According to Figures 12 and 13, increasing the dimensionless frequency results in an increase in the amount of vibration and amplitude in all of the graphs. In (a) group of Figures 12 and 13, graphs are symmetric due to the perpendicular wave front. According to the preliminary assumption, incident waves propagation is from negative x/b to

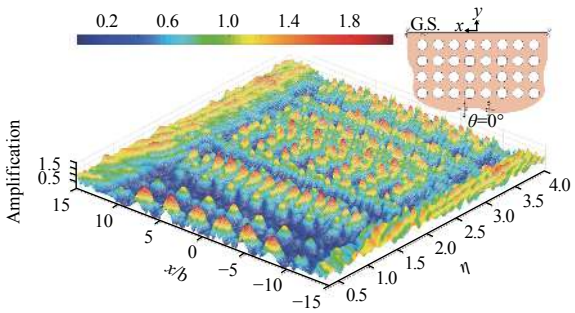

Figure 11 3-D amplification of the ground surface versus different dimensionless frequencies for the model of 32 circular cavities subjected to SH-waves and the incident angle of θ=0°

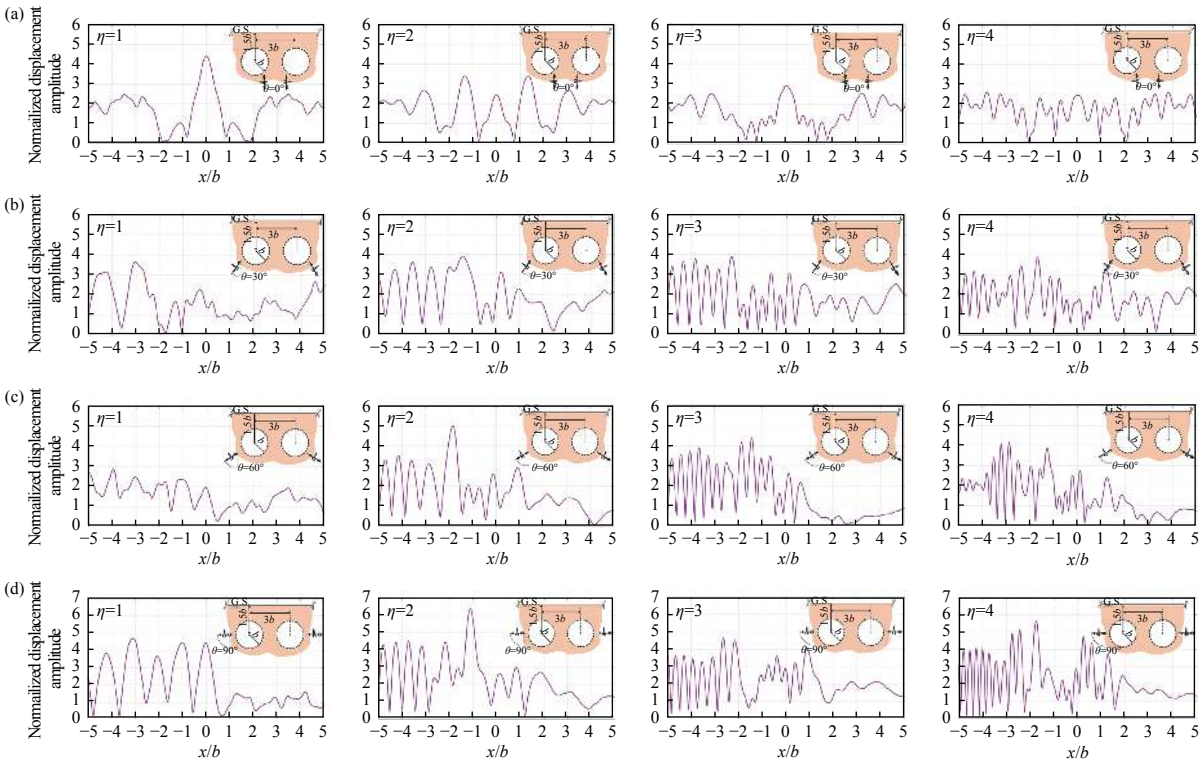

Figure 12 Normalized displacement amplitude of the ground surface versus x/b for the model of two cavities with the radius of b in the depth of d=1.5b subjected to SH-waves and the incident angles of (a) θ=0°, (b) θ=30°, (c) θ=60°, and (d) θ=90° for different dimensionless frequencies

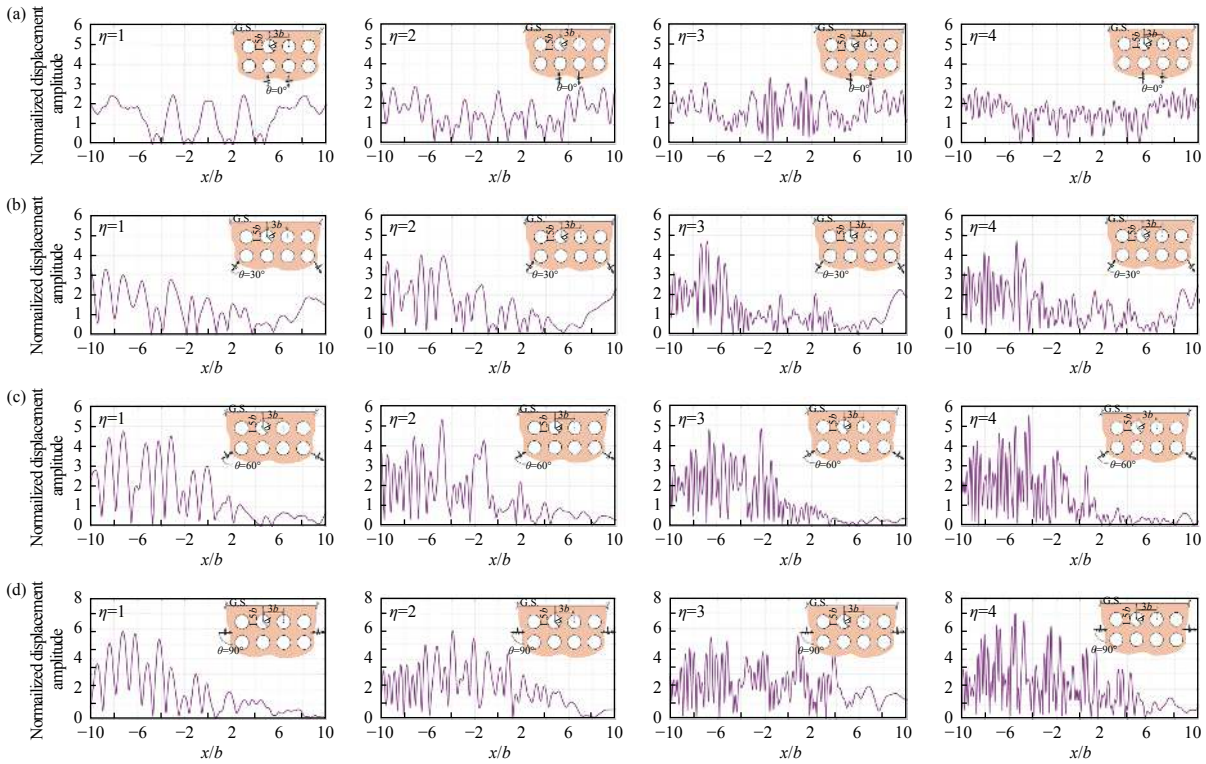

Figure 13 Normalized displacement amplitude of the ground surface versus x/b for the model of eight cavities with the radius of b in the depth of d=1.5b subjected to SH-waves and the incident angles of (a) θ=0°, (b) θ=30°, (c) θ=60°, and (d) θ=90° for different dimensionless frequencies

the positive side. Because of the diffraction and collision of waves with cavities, when the wave front is angled, incoming waves are compressed behind the cavities where the higher values of normalized displacement amplitude are obtained. For the model of two cavities, the highest value of amplitude is recorded to be 6 for the incident angle of 90°. Moreover, for the model of eight cavities, the highest recorded value is more than 7 at the same condition. Hence, higher amplitudes are expected for the greater number of cavities. For higher η values, the corresponding amplitudes are also higher. Alternatively, when the angle of wave front approaches the horizontal mode, the amplitude values show a greater increase and more complexity. Due to the arrangement of the cavities, when the incident wave angle is 90°, the wave's path through the cavities provides more diffraction around the cavities with more revealed responses.

Comparing Figures 11 and 14, low amplitudes are observed especially in η values of 1, 1.9, and 3.5 in the 3-D shape. The main reason for these low valley-shaped amplitudes is the intrinsic normalized Fourier amplitude of the Ricker wavelet. In fact, the small variations of the frequency lead to large changes in amplitude values that emerge as the low amplifications corresponding to the mentioned values of η.

Figure 15 represents the amplifications in three selected points by illustrating the response of ground surface versus the dimensionless periods for the model of two cavities. The dimensionless period parameter is the reverse of the dimensionless frequency. This figure shows how the different angles of incident waves affect the amplification of the ground surface response. For the incident angle of 0°, the amplifications of points (1) and (3) are coincident. Comparing the results of 0° with those of other incident angles indicates that, when the angle of the wave front increases, higher vibrations are achieved in lower values of dimensionless period. Besides, by increasing the dimensionless period, lower vibrations are revealed on the graphs. For the incident angle of 0°, the amplification of the ground surface in the area between cavities is higher than that of other points because of the trapped waves, leading to a 2.4-time waves amplification. The highest amplification value is obtained as about 2.9 for the incident angle of 90°. As mentioned before, when the wave front is horizontal, the existence of cavities against the incident wave's path leads to the compressing and amplification of the waves behind the collision point. Inversely, for point (3) placed behind the wave's front, the lowest results of amplification are achieved because the waves were not allowed to reach the other side.

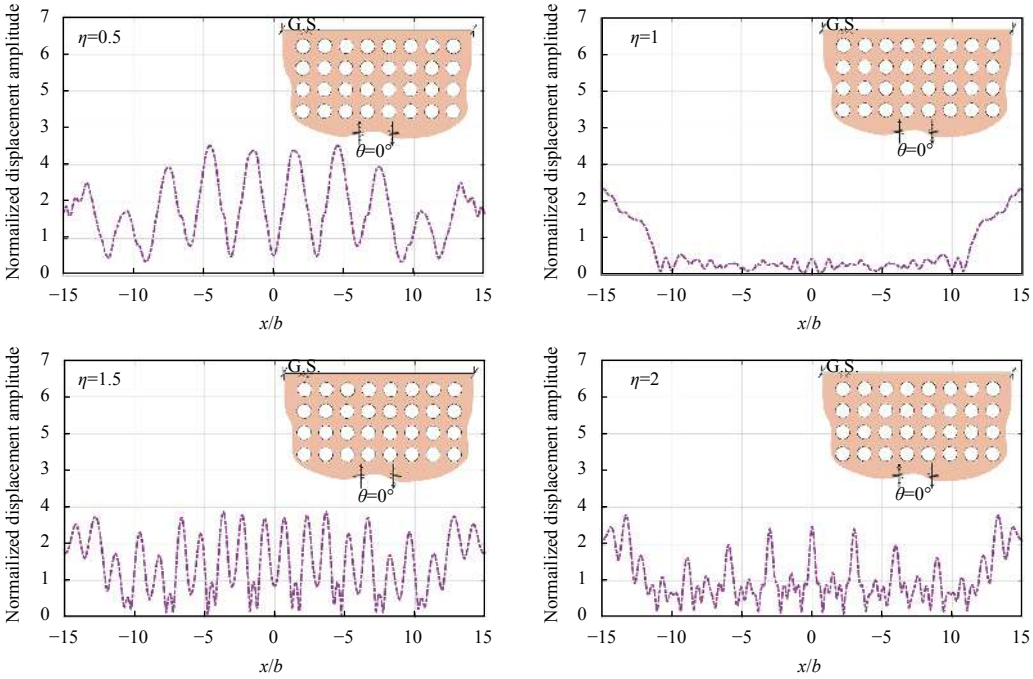

Figure 14 Normalized displacement amplitude of the ground surface versus x/b for the model of 32 cavities with the radius of b in the depth of d=1.5b subjected to SH-waves and the incident angle of θ=0° for different dimensionless frequencies

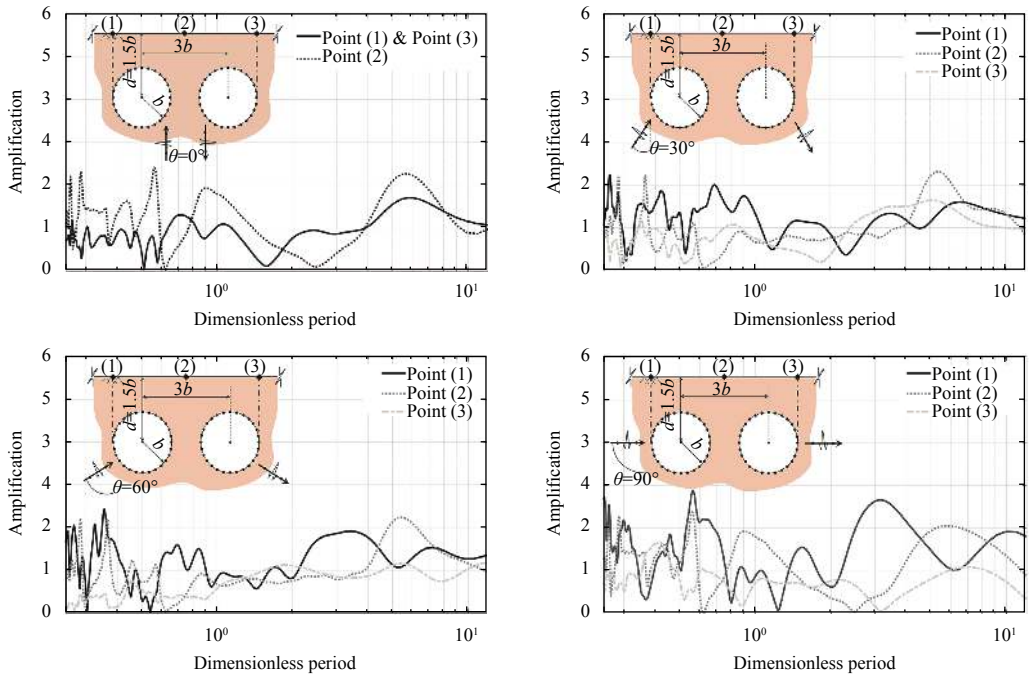

Figure 15 Amplification of the ground surface versus dimensionless period for the model of two cavities with the radius of b in the depth of d=1.5b subjected to SH-waves and the incident angles of (a) θ=0°, (b) θ=30°, (c) θ=60°, and (d) θ=90°

8 Conclusions

The time-domain responses of the ground surface presented for a linear elastic half-plane including regularly distributed enormous embedded circular cavities subjected to propagating obliquely incident plane SH-waves were obtained. A predefined approach known as the half-plane time-domain BEM was developed for this purpose. The method was able to focus the meshes only around the cavities. After applying the method for each cavity and

obtaining the influence coefficients of the matrices, an attached matrix was achieved to obtain the boundary values for the displacement fields. The ground surface displacements were also determined by defining the internal points as source nodes. A verification example was solved and the results were compared with the literature. The results revealed that the method is appropriate for the seismic analysis of problems with complex geometries. Then, an advanced numerical study was performed to obtain the ground surface response in the presence of enormous cavities. By increasing the number of cavities from 1 to 512, the time-history responses of the surface were presented. Eventually, the 3D amplification patterns of the surface were illustrated to show the frequency responses in some cases.

As a cavity was able to affect the response of the ground, the presence of enormous cavities can also change the behavior of the surface. According to the results, the effect of the presence of even one cavity was reflected on the diffraction and dispersion of the waves arrived to the surface. By increasing the number of cavities, the duration of time continuity was subsequently increased for the trapped waves, so that convergence occurred in the upper periods. The patterns of amplification in the frequency-domain show that effect of seismic isolation observed in the single cavity case (Panji et al., 2014b) is not clearly obtained in the case of enormous cavities, and the surface always encounters intermittent oscillations. The results of the present paper can be used to identify the behavior of dry porous media as well as composite materials.

References

Ahmad S and Banerjee PK (1988) Multi-domain BEM for two-dimensional problems of elastodynamics. Int J Numer Meth Eng **26**(4): 891–911

Aki K (1993) Local site effects on weak and strong ground motion. Tectonophysics **218**(1-3): 93-111.

Alyagshi EMN and Sandhu RS (1987) A parametric study of the finite element eigenfunction method for the scattering of SH-waves. Soil Dyn Earthq Eng **6**(2): 70–74

Antonio J and Tadeu A (2001) 3-D scattering by multiple cylindrical cavities buried in an elastic formation. Eur J Mech A/Solids **20**: 367–383

Ausilio E, Conte E and Dente G (2008) Seismic response of alluvial valleys to SH-waves. In: Seism Eng Conf. AIP Conf. Proc. 1020(1): 199–206

Avila-Carrera R, Sanchez-Sesma FJ and Aviles J (2008) Transient response and multiple scattering of elastic waves by a linear array of regularly distributed cylindrical obstacles: anti-plane *S*-wave analytical solution. Geofis Int **47**(2): 115–126

Balendra T and Thambiratn DP (1984) Dynamic response of twin circular tunnels due to incident SH-waves. Earthq Eng Struct Dyn **12**: 181–201

Belytschko T and Chang HS (1988) Simplified direct time integration boundary element method. J Eng Mech **114**(1): 117–134

Benites R, Aki K and Yomigida K (1992) Multiple scattering of SH-waves in 2-D media with many cavities. Pure appl Geophys **138**: 353–390

Benites R, Roberts PM, Yomogida K and Fehler M (1997) Scattering of elastic waves in 2-D composite media I. Theory and test. Phys Earth planet Int **104**: 161–173

Beskos DE (1987) Boundary element methods in dynamic analysis. Appl Mech Rev **40**(1): 1–23

Beskos DE (1997) Boundary element methods in dynamic analysis: part II (1986–1996). Appl Mech Rev **50**(3): 149–197

Brebbia CA and Dominguez J (1989) Boundary Elements: An Introductory Course. Boston: Comp Mech Pub. Southampton; 1989

Datta SK and El-Akily N (1978) Diffraction of elastic waves in a half-space. I. Integral representation and matched asymptotic expansions. In: Modern Problems in Elastic Wave Propagation. New York: Wiley-Interscience. 197–218

Datta SK and Shah AH (1982) Scattering of SH-waves by embedded cavities. Wave Motion **4**: 265–283

Do N, Dias D, Oreste P and Djeran-Maigre I (2015) 2-D numerical investigation of segmental tunnel lining under seismic loading. Soil Dyn Earthq Eng **72**: 66–76

Dominguez J (1993) Boundary Elements in Dynamics. Comp Mech Pub, Southampton, Boston

Dravinski M and Yu MC (2011) Scattering of plane harmonic SH-waves by multiple inclusions. Geophys J Int **186**: 1 331–1 346

Dravinski M (1983) Ground motion amplification due to elastic inclusions in a half-space. Earthq Eng Struct Dyn **11**: 313–335

Dravinski M (1982) Influence of interface depth upon strong ground motion. Bull Seismol Soc Amer **72**(2): 597–614

England R, Sabina FJ and Herrera I (1980) Scattering of SH-waves by surface cavities of arbitrary shape using boundary methods. Phys Earth Planet Inter **21**: 148–157

Faik Kara H (2016) Diffraction of plane SH-wave by a cylindrical cavity in an infinite wedge. World multidiscip civil eng-archit, urban planning symposium. Procedia Eng **161**: 1 601–1 607

Foldy LL (1984) The multiple scattering of waves I. General theory for isotropic, scattering by randomly distributed scatters. Phys Rev **67**: 107–119

Hadley PK, Askar A and Cakmak AS (1989) Scattering of waves by inclusions in a nonhomogeneous elastic half space solved by boundary element methods. Technical Report: NCEER-89-0027, 1989

Hirai H (1988) Analysis of transient response of SH-wave scattering in a half-space by the boundary element method. Eng Anal **5**(4): 189–194

Huang J, Dua X, Zhaoa M and Zhaoa X (2017) Impact of incident angles of earthquake shear (S) waves on 3-D non-linear seismic responses of long lined tunnels. Eng Geol **222**: 168–185

Israil ASM and Banerjee PK (1990a) Advanced development of

time-domain BEM for two-dimensional scalar wave propagation. Int J Numer Methods Eng **29**(5): 1 003–1 020

Israil ASM and Banerjee PK (1990b) Advanced time-domain formulation of BEM for two-dimensional transient elastodynamics. Int J Numer Methods Eng **29**(7): 1 421–1 440

Kattis SE, Polyzos D and Beskos DE (1999) Vibration isolation by a row of piles using a 3-D frequency-domain BEM. Int J Numer Meth Eng **46**: 713–728

Kawase H (1988) Time-domain response of a semi-circular canyon for incident SV, P and Rayleigh waves calculated by the discrete wave-number boundary element method. Bull Seismol Soc Amer **78**(4): 1 415–1 437

Keller JB (1962) Geometrical Theory of Diffraction. J Opt Soc Am **52**: 116–130

Kikuchi M (1981a) Dispersion and attenuation of elastic waves due to multiple scattering from inclusions. Phys Earth planet Inter **25**: 159–162

Kikuchi M (1981b) Dispersion and attenuation of elastic waves due to multiple scattering from cracks. Phys Earth planet Inter **27**: 100–105

Lax M (1951) Multiple scattering of waves. Revs Modern Phys **23**: 287–310

Lee VW and Trifunac MD (1979) Response of tunnels to incident SH-waves. J Eng Mech Div **105**(4): 643–659

Lee VW (1977) On the deformations near circular underground cavity subjected to incident plane SH-waves. In: Conference Proceedings of application of Computer Methods in Engineering. Los Angeles: Uni of South California. 9: 51–62

Li P and Song E (2015) Three-dimensional numerical analysis for the longitudinal seismic response of tunnels under an asynchronous wave input. Comp Geotech **63**: 229–243

Liang J, Ba Z and Lee VW (2007) Diffraction of plane SV-waves by an underground circular cavity in a saturated poroelastic half-space. ISET J Earthq Tech **44**(2): 341–375

Liang J and Liu Z (2009) Diffraction of plane SV-waves by a cavity in poroelastic half-space. Earthq Eng Eng Vib **8**(1): 29–46

Liang J, Luo H and Lee VW (2010) Diffraction of plane SH-waves by a semi-circular cavity in half-space. Earthq Sci **23**(1): 5–12

Liang J, Zhang H and Lee VW (2003) A series solution for surface motion amplification due to underground twin tunnels: Incident SV-waves. Earthq Eng Eng Vib **2**(2): 289–298

Liang J, Zhang H and Lee VW (2004) A series solution for surface motion amplification due to underground group cavities: Incident P-waves. Acta Seismologica Sinica **17**(3): 296–307

Lin H and Liu DK (2002) Scattering of SH-wave around a circular cavity in a half-space. Earthq Eng Eng Vib **22**: 9–16

Liu Q, Zhang C and Todorovska MI (2016) Scattering of SH-waves by a shallow rectangular cavity in an elastic half space. Soil Dyn Earthq Eng **90**: 147–157

Liu Q, Zhao M and Zhang C (2014) Antiplane scattering of SH-waves by a circular cavity in an exponentially graded half space. Int J Eng Sci **78**: 61–72

Luco JE and de Barros FCP (1994) Dynamic displacements and stresses in the vicinity of a cylindrical cavity embedded in a half-space. Earthq Eng Struct Dyn **23**: 321–340

Luo H, Lee VW and Liang J (2010) Anti-plane SH-waves diffraction by an underground semi-circular cavity: analytical solution. Earthq Eng Eng Vib **9**(3): 385–396

Mow CC and Pao YH (1971) The diffraction of elastic waves and dynamic stress concentrations. Rand Corp Santa Monica Calif. R-482-PR; 1971

Ohtsu M and Uesugi S (1985) Analysis of SH-wave scattering in a half space and its applications to seismic responses of geological structures. Eng Anal **2**(4): 198–204

Panji M and Ansari B (2017a) Modeling pressure pipe embedded in two-layer soil by a half-plane BEM. Comp Geotech **81**: 360–367

Panji M and Ansari B (2017b) Transient SH-wave scattering by the lined tunnels embedded in an elastic half-plane. Eng Anal with Boundary Elements **84**: 220–230

Panji M, Asgari Marnani J and Tavousi TS (2011) Evaluation of effective parameters on the underground tunnel stability using BEM. J Struct Eng Geotech **1**(2): 29–37

Panji M, Kamalian M, Asgari Marnani J and Jafari MK (2013a) Amplification pattern of semi-sine shaped valleys subjected to vertically propagating incident SH-waves. Comp Methods in Eng. Isfahan Uni of Tech (IUT), Isfahan: Iran; 2013

Panji M, Kamalian M, Asgari Marnani J and Jafari MK (2014a) Analysing seismic convex topographies by a half-plane time-domain BEM. Geophys J Int **197**(1): 591–607

Panji M, Kamalian M, Asgari Marnani J and Jafari MK (2014b) Antiplane seismic response from semi-sine shaped valley above embedded truncated circular cavity: a time-domain half-plane BEM. Int J Civil Eng **12**(2 and B): 160–173

Panji M, Kamalian M, Asgari Marnani J and Jafari MK (2013b) Transient analysis of wave propagation problems by half-plane BEM. Geophys J Int **194**: 1 849–1 865

Panji M, Koohsari H, Adampira M, Alielahi H and Asgari Marnani J (2016) Stability analysis of shallow tunnels subjected to eccentric loads by a boundary element method. J Rock Mech Geotech Eng **8**: 480–488

Panji M (2013) Seismic analysis of topographic features subjected to SH-waves by a half-Plane time-domain BEM [Dissertation]. Islamic Azad Uni. Sci and Res Branch. Tehran. Iran; 2013

Parvanova SL, Dineva PS, Manolis GD and Kochev PN (2014a) Dynamic response of a solid with multiple inclusions under anti-plane strain conditions by the BEM. Comp Struct **139**: 65–83

Parvanova SL, Dineva PS and Manolis GD (2013) Dynamic behavior of a finitesized elastic solid with multiple cavities and inclusions using biem. Acta Mech **224**: 597–618

Parvanova SL, Dineva PS and Manolis GD (2014b) Elastic wave fields in a half-plane with free-surface relief. Tunnels and multiple buried inclusions. Acta Mech **225**(7): 1 843–1 865

Parvanova SL, Manolis GD and Dineva PS (2015) Wave scattering by nanoheterogeneities embedded in an elastic matrix via BEM. Eng Anal with BE **56**: 57–69

Reinoso E, Wrobel LC and Power H (1993) Preliminary results of the modeling of the Mexico City valley with a two-dimensional boundary element method for the scattering of SH-waves. Soil Dyn Earthq Eng **12**(8): 457–468

Rice JM and Sadd MH (1984) Propagation and scattering of SH-

waves in semi-infinite domains using a time-dependent boundary element method. J Appl Mech **51**: 641–645

Robert S, Conoir JM, Franklin H and Lupe F (2004) Resonant elastic scattering by a finite number of cylindrical cavities in an elastic matrix. Wave Motion **40**: 225–239

Sánchez-Sesma FJ, Palencia VJ and Luzón F (2002) Estimation of local site effects during earthquakes: An overview. ISET J Earthq Tech **39**(3): 167–193

Sheikhhassani R and Dravinski M (2014) Scattering of a plane harmonic SH-wave by multiple layered inclusions. Wave Motion **51**: 517–532

Smerzini C, Aviles J, Sanchez-Sesma FJ and Paolucci R (2008) Effect of underground cavities on surface earthquake ground motion under SH-wave propagation. Earthq Eng Struct Dyn **38**(12): 1 441–1 460

Trifunac MD (1973) Scattering of plane SH-waves by a semi cylindrical canyon. Earthq Eng Struct Dyn **3**(1): 267–281

Twersky V (1962) Multiple scattering by arbitrary configuration in three dimensions. J Math Phys **3**: 83–91

Twersky V (1952) Multiple scattering of radiation by an arbitrary planar configuration of parallel cylinders and by two parallel cylinders. J Appl Phys **23**: 407–414

Varadan VK, Varadan VV and Pao YH (1978) Multiple scattering of elastic waves by cylinders of arbitrary cross section. I. SH-waves. J Acoust Soc Am **63**: 1310–1319

Wang G and Liu D (2002) Scattering of SH-wave by multiple circular cavities in half-space. Earthq Eng Eng Vib **1**(1): 36–44

Wang X and Sudak LJ (2007) Scattering of elastic waves by multiple elastic circular cylinders with imperfect interface. Waves Rand Media **17**: 159–187

Wong HL and Jennings PC (1975) Effects of canyon topography on strong ground motion. Bull Seismol Soc Amer **65**(5): 1 239–1 257

Yang RB and Mal AK (1994) Multiple scattering of elastic waves in a fiber-reinforced composite. J Mech Phys Solids **42**: 1 945–1 968

Yomogida K, Benites R, Roberts PM and Fehler M (1997) Scattering of elastic waves in 2-D composite media II. Waveforms and spectra. Phys Earth Planet Inter **104**: 175–192